Greener Processes in the Preparation of Thin Film Nanocomposite Membranes with Diverse Metal-Organic Frameworks for Organic Solvent Nanofiltration

Lorena Paseta[a], Marta Navarro[a], Joaquín Coronas[a,b], Carlos Téllez[a,b,]*

[a]Instituto de Nanociencia de Aragón (INA) and Chemical and Environmental Engineering Department, Universidad de Zaragoza, 50018 Zaragoza, Spain.

[b]Instituto de Ciencia de Materiales de Aragón (ICMA), CSIC-Universidad de Zaragoza, 50018 Zaragoza, Spain

[*]Corresponding author: ctellez@unizar.es

ABSTRACT: The toxic solvent dimethylformamide have been replaced by the greener dimethylsulfoxide in the casting and activation processes for the preparation of thin film composite (TFC) membranes. This methodology has been validated with the use of MOFs ZIF-8, ZIF-93 and UiO-66 as fillers for thin-film nanocomposite (TFN) membranes. These membranes were successfully applied in the organic solvent nanofiltration of sunset yellow (SY) in methanol obtaining the highest permeance when UiO-66 and ZIF-93 were used with a value of 11 $L \cdot m^{-2} \cdot h^{-1} \cdot bar^{-1}$. The permeance improvements are related to the MOF porosity, polyamide-MOF layer thickness and the hydrophilic/hydrophobic character of the membrane.

KEYWORDS: Greener preparation process, Organic Solvent Nanofiltration, Thin Film Nanocomposite, Metal-organic frameworks.

1. INTRODUCTION

Nanofiltration is a membrane separation process for liquids characterized by an operating pressure difference ranging from 5 to 40 bar and a molecular weight cut-off (MWCO) between 200 and 1000 Da [1]. While this technique has been widely used in water treatment processes [2-4], it has recently received much attention for its application with organic solvents, the so-called organic solvent nanofiltration (OSN) process, with important economic, environmental and safety benefits [1,5].

The most competitive membranes in OSN are the so-called thin film composite (TFC) membranes, first developed by Cadotte [6]. Although, thin film nanocomposite membranes (TFN, i.e. including fillers in the TFC membrane), first developed by Jeong et al. [7] for reverse osmosis, have also been widely used for OSN [5,8] obtaining an improvement in permeance without sacrificing rejection in comparison with TFC membranes. Nowadays several different nanoparticles are also used as fillers, namely TiO_2 [9-11], MCM-41 silica [12], graphene oxide [13] and a limited range of metal-organic frameworks (MOFs) [14-16]. The foregoing is related to the tendency of modification and improvement of the thin film membrane as well as the synthesis and applications related to the MOF [17-19].

The main drawback in the fabrication of TFN membranes is that the polymer necessary to prepare the support is usually soluble in highly toxic organic solvents, such as N,N-dimethylformamide (DMF), N-methyl-2-pyrrolidone (NMP) or N,N-dimethylacetamide (DMAc) [20]. Moreover, in the case of TFC and MOF-TFN membranes, DMF is commonly used in the post-treatment as an activating solvent (either by bath, filtration

or a combination of both treatments) [16,21-22]. In recent years, the principles of Green Chemistry are implanting [23] focusing on resource efficiency, nontoxicity and the environmentally friendly profile of solvents, and on the overall life cycle assessment of the product or process [24].

Solvent selection guides, in particular Sanofi's [25], provide relevant information and rankings of commonly used solvents based on several features that must be considered when designing a “green” membrane. Health issues of solvents (acute, long-term and single target organ toxicity) are evaluated by REACH (Registration, Evaluation, Authorisation and Restriction of Chemical substances) and, in particular, DMF, DMAc and NMP are classified as substances of very high concern (SVHC) in a list that is updated twice a year [26]. Given other disadvantages of DMF such as corrosivity, a melting point at 18 °C and the formation of dimethylsulfide, REACH has proposed DMSO as an advisable substitute because of its low toxicity for human health. In turn, Sanofi classified DMSO as “substitution advisable” in contrast with DMF classified as “substitution requested”.

However, very few publications have presented strategies for reducing the impact of membrane production. Of these, da Silva Burgal et al. [27] used poly(ether ether ketone), a chemical resistant polymer that does not require cross-linking and dissolves in solvents that can be easily neutralized by water. Hua et al. [28] carried out the synthesis of the selective layer using water as the reaction medium instead of hexane. Figoli et al.[29] described many successful cases were DMSO was applied for the preparation of membranes. In particular, Soroko et al. [30]. developed a new route to synthesize TFC OSN membranes using DMSO as a polyimide (PI) solvent instead of DMF and Jimenez Solomon et al. [22] used DMSO as the activating solvent for TFC membrane post-treatment instead of DMF. DMSO and DMF are considered to be

interchangeable because of their similar Hansen solubility parameters and ability to dissolve both polyimide and polyamide [29]. Furthermore, DMSO is the most environmentally friendly solvent among other PI diluents (DMF and NMP) in terms of its emissions and resource use. All these solvents were produced through the "methanol route". Capello et al. [31] showed their Life Cycle Assessment and energy profiles, obtained by the Cumulative Primary Energy Demand (CED). DMF is produced in two steps requiring between 50 and 100 MJ-eq per kg of product. NMP requires four production steps and between 100 and 150 MJ-eq per kg of product. In contrast, DMSO is produced in only one step and causes the lowest CED with less than 50 MJ-eq per kg of product.

Our aim for a more sustainable nanofiltration process is to design greener processes for membrane preparation but also to achieve membranes able to resist and filter organic solvents. Here, we report the preparation of TFC and MOF-TFN membranes using DMSO, a greener solvent than traditional ones, both to dissolve the polymer and to activate the membrane. In addition, continuing with the development of MOFs as fillers in TFN membranes, we have incorporated ZIF-8 and two other MOFs that to date have not been used as fillers in OSN: ZIF-93 and UiO-66. These MOFs (see their structure and composition in Figure 1a) differ in their pore size and hydrophilicity and provide the membrane with different performances in OSN applications.

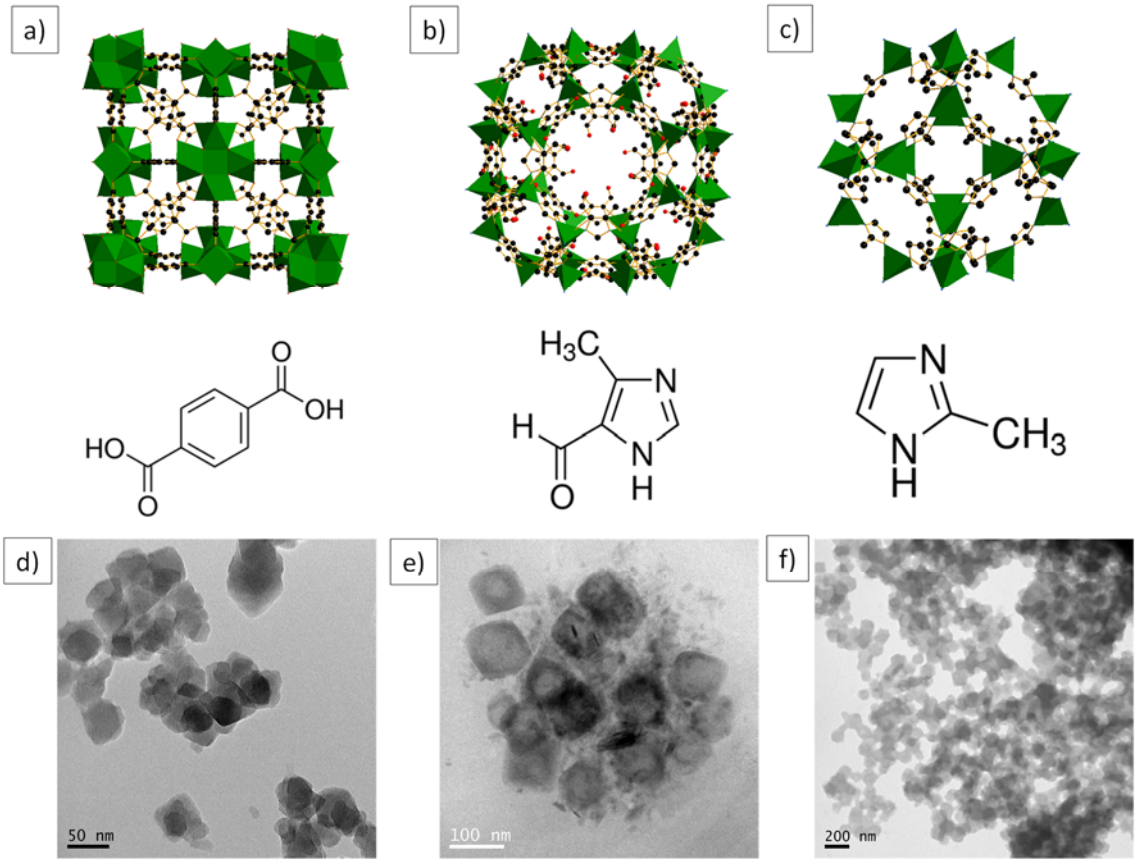

Figure 1: a) Building blocks of UiO-66 with the $Zr_6O_4(OH)_4$ clusters in green and chemical structure of the terephthalic acid, **b)** Building blocks of ZIF-93 with the ZnN_4 tetrahedra in green and chemical structure of the 4-methyl-5-imidazolecarboxaldehyde linker and **c)** Building blocks of ZIF-8 with the ZnN_4 tetrahedra in green and chemical structure of the 2-methylimidazole linker. Oxygen, nitrogen and carbon atoms are in red, blue and black, respectively. These structures were made with Diamond 3.2 using the corresponding CIF files [32-34]. **d, e, f)** TEM images of **d)** UiO-66, **e)** ZIF-93 and **f)** ZIF-8.

2. MATERIAL AND METHODS

2.1. MOFs preparation

The syntheses of ZIF-93 [35], ZIF-8 [36] and UiO-66 [37] were carried out as previously reported. The detailed procedures can be found in the Supporting Information.

2.2. Preparation of PI supports

The PI supports were prepared as follows: a dope solution of 24% (w/w) was prepared by dissolving P84® (HP polymer GmbH) in DMSO (99.5%, Scharlab) and stirring overnight. Once all the air bubbles disappeared, the solution was cast on a polypropylene non-woven backing material at a casting speed of 0.04 $m \cdot s^{-1}$ using a casting knife set (Elcometer 4340 Automatic Film Applicator) at a thickness of 250 μm. Immediately after casting, the membrane was immersed in a deionized water bath at 23 °C, where the phase inversion occurred for 10 min. The membrane supports were transferred to a fresh water bath and left for 1 h. The wet membranes were then immersed in two consecutive baths of isopropyl alcohol (IPA – 99.5%, Scharlab) of 1 h each to remove any residual water or DMSO. Afterwards, the supports were cross-linked immersing them in a 120 $g \cdot L^{-1}$ solution of hexanediamine (HDA – 98%, Sigma Aldrich) in IPA for 16 h at 20 °C. Next, the membranes were washed four times with IPA for 1 h each to remove any trace of HDA. Finally, the supports were immersed in a solution with a 3:2 volume ratio of polyethylene glycol (PEG – synthesis grade, Scharlab): IPA overnight to prevent the pores from collapsing during the IP reaction.

2.3. Preparation of TFC and TFN membranes

The ultrathin layer was formed on the cross-linked PI P84® supports by interfacial polymerization. First, two solutions were prepared: an aqueous solution of 2% (w/v) m-phenylenediamine (MPD – 99%, Sigma-Aldrich) and a solution of 0.1% (w/v) trimesoyl chloride (TMC – 98%, Sigma-Aldrich) in hexane (extra pure, Scharlab). Afterwards, a 60 cm^2 support was placed in a glass filtration holder for the interfacial polymerization reaction and 30 mL of the aqueous solution was added. After 2 min, the excess solution was removed and the membrane surface was dried with tissue paper. Next, 30 mL of the TMC solution was added and left for 1 min. After that, 10 mL of hexane was poured to

stop the reaction, the excess was removed and an extra 10 mL of hexane was added to remove unreacted TMC. Finally, 10 mL of water was added to wash out the hexane and the TFC membrane formed was stored in deionized water in the fridge. In the case of the TFN membranes, the fabrication procedure was the same overall as for TFC but dispersing 0.2% (w/v) of MOF in the organic phase before the IP reaction.

Prior to the nanofiltration process, the membranes were treated with two different post-treatment procedures. In the first one, the membrane was placed in a 10 min solvent bath at room temperature. The second post-treatment procedure, carried out after the first has been done, consisted of 10 min filtration with solvent at 20 bar of feed pressure and at room temperature, using the same filtration module as for OSN. In both post-treatment procedures, DMF or DMSO were used as solvents to compare the substitution of DMF for the greener solvent DMSO.

2.4. Material characterization

The crystallinity of the MOF nanoparticles was determined by powder X-ray diffraction (XRD), performed at room temperature in an Empyrean PANalytical diffractometer with a Cu-K_α radiation source (λ=1.5406 Å). Data were collected in the 2θ range from 2.5° to 40° and at a scanning rate of 0.01°·s^{-1}. Thermogravimetric analyses (TGA) were carried out in a Mettler Toledo TGA/SDTA 851e in order to check if the MOF nanoparticles were properly activated. The powder samples were put in 70 µL alumina pans and heated up to 700 °C with a heating rate of 10 °C·min^{-1} under air atmosphere. The specific surface area and pore volume of the synthesized ZIF-8, ZIF-93 and UiO-66 nanoparticles were obtained using a Micromeritics Tristar 3000 at 77 K. The ZIF-93 and ZIF-8 samples were first degassed at 200 °C for 8 h and the UiO-66 nanoparticles at 100 °C for 8 h. Their specific surface areas were calculated by the Brunauer–Emmett–Teller (BET) method and the pore volume at a relative pressure of P/P_0=0.98.

Scanning electron microscopy (SEM) images of the MOF crystals and of the surface and cross-section of the membranes were obtained using an Inspect-F20 microscope (FEI) operated at 10 kV. The samples were prepared over a magnetic strip and coated with platinum under vacuum conditions. Membrane cross-sections were prepared by freeze-fracturing in liquid N_2. In order to measure the PA-MOF thickness layer, a TFN membrane for each MOF was synthetized over a non-crosslinked P84® support without backing material. Then, these membranes were immersed in N,N-dimethylformamide at room temperature for 5 min to dissolve the P84® support. The separated PA top layer was placed onto a carbon mesh grid and observed by SEM.

In the last stage of the interfacial polymerization process, a fragment of the PA film combined with each MOF was detached from the polyimide support, removed from the distilled water bath and placed onto a carbon mesh grid. Transmission Electron Microscopy (TEM) was then performed on this sample prepared ad hoc using a FEI Tecnai T20, operated at 200 kV, in order to check the distribution of the MOF nanoparticles within the TFN membrane and their crystallinity. This technique was also used to characterize the MOF nanoparticles.

Quantitative surface roughness analysis of the TFC membranes post-treated with a DMF or DMSO bath was carried out using atomic force microscopy (AFM), at a resonant frequency of 300 kHz with a force constant of 40 mN, and a silicon cantilever provided by Bruker. The AFM device was a Veeco MultiMode 8 scanning probe microscope in tapping mode. Images were recorded from 6 and 12 μm^2 of the areas of the TFC-DMSO and TFC-DMF membranes, respectively, at a scan rate of 1 Hz, an amplitude set-point lower than 1 V and under ambient conditions. After the measurement, the average plane roughness (R_a) and the root mean square (*RMS*) were obtained. Contact angle measurements were performed using a Krüss DSA 10 MK2 at

20 °C. At least 3 measurements were carried out in the TFC and TFN membranes post-treated with a DMF or DMSO bath to obtain an average value for each membrane.

To detect the presence of MOFs, the TFN membranes were characterized by Attenuated Total Reflection Fourier Transform Infrared Spectroscopy (ATR-FTIR) and their spectra were compared with reference MOF-powder samples and the TFC membranes, subtracting the spectrum of the TFC from the TFN membrane. The spectra were recorded in the 600-4000 cm^{-1} wavenumber range with an accuracy of 4 cm^{-1}, using a Bruker Vertex 70 FTIR spectrometer equipped with a deuterated triglycine sulfate detector and a Golden Gate diamond ATR accessory. Moreover, the metal quantity in the TFN-MOF membranes was determined by X-ray photoelectron spectroscopy (XPS, AXIS Ultra DLD system from Kratos Analytical), using monochromated Al K_α (1486.6 eV) excitation radiation at 15 kV, 15 mA and power of 225 W. The obtained metal% was related with the quantity of metal in the MOF through its empirical chemical formula. Ar^+ bombardment was performed before measurement and then the concentration of Zn or Zr was profiled, etching the sample from the top with a beam energy of 3 keV and 5 mA at different time intervals. The peaks were fitted using the software CasaXPS.

In order to check the crosslinking extent and chemical stability of the TFC membranes, their gel content was calculated. For that purpose, the TFC membranes were soaked for two weeks in the corresponding activating solvent (DMF or DMSO). Afterwards, the sample was gently dried with tissue paper. To average the values, the experiment was repeated three times with fragments of the same sample. The gel content (GC) was determined using the following equation:

$$GC = \left(\frac{M_{wet}}{M_{dry}}\right) \ (Eq. 1)$$

where M_{wet} is the weight of the TFC membrane after being soaked in DMF or DMSO and gently dried, and M_{dry} is the initial weight of the TFC membrane.

2.5. Membrane performance

The nanofiltration process was performed in a dead-end membrane module (Sterlitech HP4750). The performance of the membranes was evaluated using a feed of 20 $mg \cdot L^{-1}$ of Sunset Yellow (SY, Sigma Aldrich, 90%) in MeOH. The effective area of the membrane was 12 cm^2 and the feed volume was 250 mL. All experiments were carried out at a feed pressure of 20 bar and 23 °C. The rejection and the permeance were calculated by the following equations:

$$Permeance = \frac{V}{\Delta P \times A \times t} \left[\frac{L}{m^2 \times h \times bar}\right] \quad (Eq. 2)$$

$$Rejection\ (\%) = \left(1 - \frac{C_{permeate}}{C_{residue}}\right) \times 100 \quad (Eq. 3)$$

where V is the volume (L), A is the nanofiltration area of the membrane (m^2), t is the time for the permeate collection (h) and ΔP is the pressure difference (bar) used. Both concentrations, permeate ($C_{permeate}$) and residue ($C_{residue}$), were measured by an UV spectrometer (Jasco V-670 spectrophotometer) using water as solvent. For this purpose, once the permeance was stable, 3 mL of permeate and the residue was taken and left in the fume hood until the MeOH evaporated and was replaced by 3 mL of deionized water. The samples were measured at the wavelength of maximum absorbance for the Sunset Yellow: 480 nm. The results given correspond to the average after measuring a minimum of three membranes.

Additionally, the membrane performance was tested to evaluate the chemical resistance of the TFC and TFN membranes to a sequence of solvents without any solute.

Firstly, distilled water was filtrated for 30 min, followed by methanol, tetrahydrofuran (THF, HPLC grade, VWR International), acetone and finally distilled water again.

3. RESULTS AND DISCUSSION

3.1. MOFs characterization

The XRD patterns of the MOFs prepared in this work (Fig. S1) reveal their purity and crystalline structure after comparing them with the simulated ZIF-8, ZIF-93 and UiO-66 XRD patterns. Figure 1a-c shows the structure of these MOFs and their corresponding organic linker. The nanosized MOF crystals showed the expected morphology (Figure 1d,e,f and Fig. S2) as described in the literature [35-37] and were obtained with a narrow particle size distribution, ranging from 48 to 127 nm with a small standard deviation (9-18 nm) (Table 1). The order of particle size was UiO-66 (48 nm) < ZIF-93 (67 nm) < ZIF-8 (127 nm). Thermogravimetric analyses in air atmosphere (Fig. S3) confirm that the MOF nanoparticles were correctly activated and neither the solvent nor unreacted linkers were inside the pores. The stability of the MOFs was in the order ZIF-93, ZIF-8 and UiO-66 with the maximum mass loss rate of the polymer degradation at 393, 471 and 547 °C, respectively. Their BET specific surface areas (Table 1) were 737, 971 and 1287 $m^2 \cdot g^{-1}$ for ZIF-93, UiO-66 and ZIF-8, respectively. These values are in good agreement with the literature for UiO-66 [38] and ZIF-8 [39]. In the case of ZIF-93, the reported BET surface area in the literature was slightly higher (864 - 891 $m^2 \cdot g^{-1}$) [33], which probably corresponds to larger ZIF-93 crystals. Moreover, their uptake curves correspond to type I isotherms, typical of microporous materials (Fig. S4), and at high relative pressure the nitrogen uptake is due to capillary condensation between the nanoparticles.

Table 1. Particle size determined from the SEM images and BET area of the UiO-66, ZIF-93 and ZIF-8 synthesized in this work. The pore size (nm) is indicated as a reference.

MOF	Particle Size (nm)	BET specific surface area ($m^2 \cdot g^{-1}$)	Window aperture/cavity diameter(Å) [34,40-42]
UiO-66	48 ±9	971 ±13	6/7.5-12
ZIF-93	67 ±13	737 ±11	3.7/15.8
ZIF-8	127 ±18	1287 ±40	3.4/11.8

3.2. Comparison of TFC membranes post-treated using DMF and DMSO

TFC membranes were subjected to two different post-treatment procedures: the first with only 10 min in a solvent bath and the second one, in addition to the solvent bath, 10 min of solvent filtration, using in both cases activating solvents with similar Hildebrand solubility parameters to the polyamide top layer, namely DMF and DMSO (23 $(MPa)^{1/2}$, 24.8 $(MPa)^{1/2}$ and 26.6 $(MPa)^{1/2}$ for PA, DMF and DMSO respectively) [22]. The efficiency of these post-treatments in increasing the solvent permeance during OSN has been extensively demonstrated [14,16,21-22]. Upon exposure to these solvents, low weight polyamide fragments are supposed to dissolve unblocking flux pathways. DMSO has been proved to be an excellent alternative to DMF to elaborate and activate TFC membranes in an environmentally friendly manner [30,43], as their analogous interaction, according to the HSP calculations between them (similar Ra value) and polyimide (during P84® casting) or polyamide (during bath and filtration post-treatments) (see Table S1).

The SEM micrographs of the surface of TFC membranes post-treated with a 10 min DMF bath reveal the characteristic ridge and valley morphology of the polyamide layer (Fig. S5a) while the membranes post-treated using DMSO show the polyamide layer with a slightly more nodular structure (Fig. S5b). In any case, the polyamide layer was well formed and a difference in the post-treatment influence of the two solvents was not visible to the naked eye. Upon analysing their surface roughness, the AFM results (2D and 3D images (see Figure 2), and R_a and *RMS* values) of four different areas of the TFC membranes show a smoother surface when post-treated with DMF than with DMSO. The *RMS* roughness for the TFC-DMF membrane is found to be 26.6 ± 1.8 μm while the *RMS* value for the TFC-DMSO is slightly higher and shows a greater deviation, 39.9 ± 7.7 μm. However, the difference in their surface roughness did not provoke a difference in their hydrophobic properties, as the contact angle measurements (Table 2) were reported to be 76 ± 3° for both TFC membranes. Furthermore, the gel content parameters of the PI network post-treated with DMF or DMSO are very similar: 91.1 ±1.3 and 92.2 ±2.1, respectively. The similar hydrophobicity and gel content parameters for both PI supports are related to a similar cross-linking density of the polymer network. As has been noted, there is not significant difference between the post-treatments performed by DMF or DMSO for activating TFC membranes.

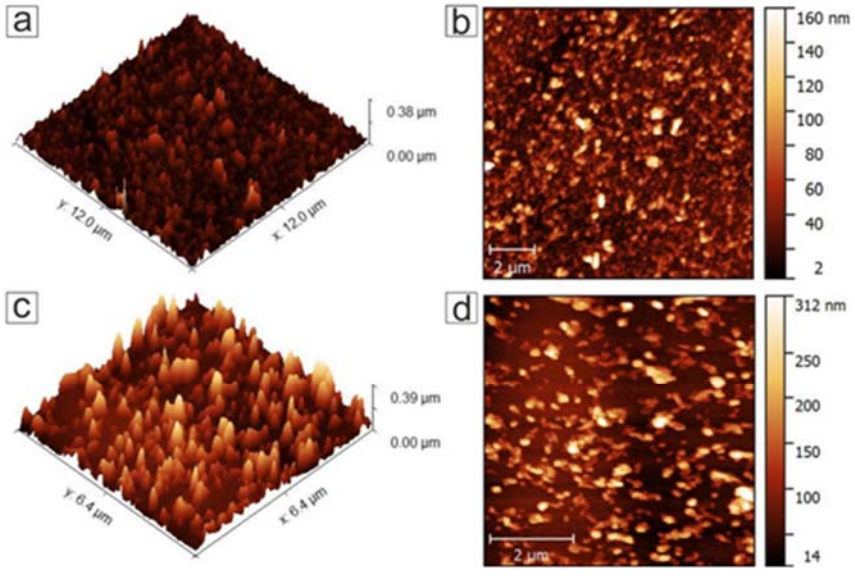

e

	R_a (µm)	*RMS* (µm)	Gel Content
TFC DMF	18.3 ± 1.1	26.6 ± 1.8	91.1 ± 1.3
TFC DMSO	31.0 ± 5.9	39.9 ± 7.7	92.2 ± 2.1

Figure 2. 3D **(a, c)** and 2D **(b, d)** AFM images of the surface of TFC membranes with a DMF **(a, b)** or DMSO **(c, d)** bath post-treatment and **e)** R_a, *RMS* and gel content values

Table 2. Contact angle measurements.

Membranes	Contact angle (°)
TFC DMF	76 ± 3
TFC DMSO	76 ± 3
TFN-ZIF-93	64 ± 4
TFN-ZIF-8	78 ± 2
TFN-UiO-66	65 ± 3

When DMF was used as the “activating” solvent, the permeance and the rejection obtained after the bath post-treatment were 2.5 $L \cdot m^{-2} \cdot h^{-1} \cdot bar^{-1}$ and 91.3 %, respectively, and after filtration post-treatment 4.4 $L \cdot m^{-2} \cdot h^{-1} \cdot bar^{-1}$ and 97%. Whereas using DMSO, these values were 3.7 $L \cdot m^{-2} \cdot h^{-1} \cdot bar^{-1}$ and 91.7% after the bath treatment and 4.7 $L \cdot m^{-2} \cdot h^{-1} \cdot bar^{-1}$ and 97.1% after filtration post-treatment (Table S2). As can be seen, the permeances and rejections obtained using DMF or DMSO as the activating solvent are similar, even a bit better for DMSO which may be related to its slightly higher roughness. Accordingly, either solvent can be used as an activating solvent, which is consistent with the results obtained by Solomon et al,[22] and which shows that a greener way to synthesize TFC is possible.

3.3. Characterization of TFN membranes

ZIF-8, ZIF-93 and UiO-66 nanoparticles were used as fillers to prepare the TFN membranes. Surface and cross-section SEM micrographs of all the TFN membranes prepared are represented in Figure 3. Nodular and ridge-and-valley morphologies from the polyamide layer are clearly seen but the dispersed fillers are difficult to differentiate. In addition, the thickness of the thin polyamide-MOF layer cannot be inferred from the cross-section images.

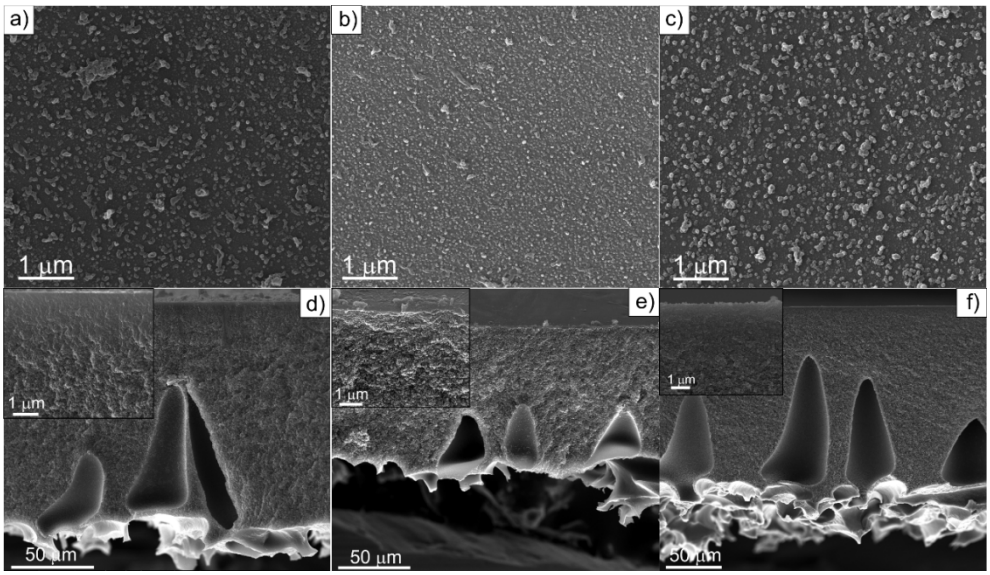

Figure 3. a-c) Surface SEM micrographs and **d-f)** cross-section SEM micrographs of the TFN membranes: **a)** and **d)** TFN-ZIF-93; **b)** and **e)** TFN-UiO-66; **c)** and **f)** TFN-ZIF-8.

In order to determine the polyamide-MOF layer thickness, samples prepared ad hoc for each MOF was observed by SEM (Figure 4). In the case of ZIF-8, the thickness of this layer was around 100 nm (Figure 4a), what it is in good agreement with the observed by Sánchez-Laínez et al. [44], whereas for both ZIF-93 and UiO-66 (Figure 4b,c) with smaller particle size, the thickness were around 35 nm. For a TFC membrane prepared in a similar way the thickness was approximately 50 nm [44].

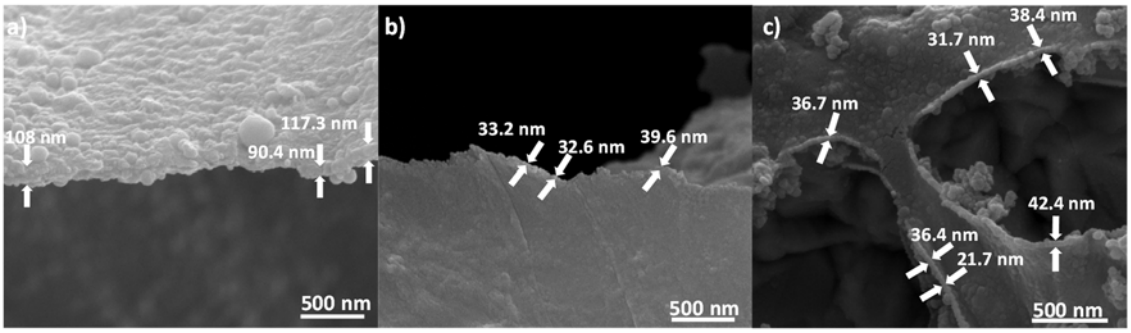

Figure 4. SEM images of the PA+MOF layer for the MOF. **a)** ZIF-8; **b)** ZIF-93 and **c)** UiO-66.

TEM images (Figure 5a, c, e) of the PA samples prepared ad hoc show how MOF nanoparticles (NPs) are dispersed inside the thin PA layer, maintaining their morphology. We can infer a similar distribution of the MOF nanoparticles in the TFN-ZIF-8 and TFN-UiO-66 membranes, although a lower coverage can be observed in the case of the TFN-ZIF-93 membrane.

XRD patterns of the TFN membranes (Fig. S6) did not reveal the presence of the MOF NPs after the IP process to form the PA thin layer because they could not diffract with sufficient intensity for their reflections to be detected, due to their low content in the composites. Therefore, the verification of the maintenance of the crystal structure of the three MOFs embedded in the PA layer after the interfacial polymerization process was performed by applying electron diffraction to the PA plus MOF samples mounted on TEM grids, as seen in Figure 5a, c, and e. Figure 5b shows the electron diffraction pattern of ZIF-8, with the spots indexed as the (310), (420), (510) and (440) diffractions (d-spacings of 5.4, 3.8, 3.3 and 3.0 Å, respectively). In addition, Figure 5d shows the electron diffraction pattern of ZIF-93, with the spots indexed as the (024), (037) and (048) diffractions (d-spacings of 6.5, 3.8 and 3.2 Å, respectively). Finally, Figure 5f displays the electron diffraction pattern of UiO-66, with the spots indexed as the (111), (222) and (333) diffractions (d-spacings of 11.9, 5.9 and 3.9 Å, respectively). The intensity of these spots was weak since the energy of the beam quickly degraded the samples and MOF NPs were included inside the amorphous PA thin film. Therefore, the crystal structure of MOF NPs seems to be maintained after the interfacial polymerization process.

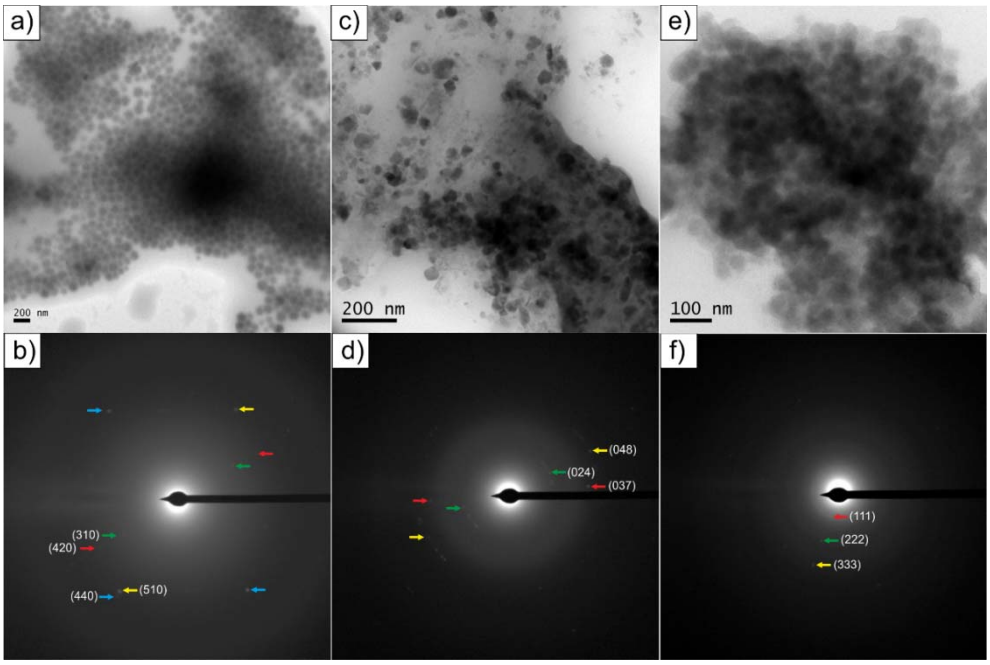

Figure 5. a, c, e) TEM images of the PA thin film with the MOFs embedded and **b, d, f)** Electron diffraction patterns of the MOFs from the previous images, indexed according to the crystal structure of: **a, b)** ZIF-8; [34] **c, d)** ZIF-93 [33] and **e, f)** UiO-66 [32]. The planes observed correspond to the MOF structure in each case. The diffraction spots are pointed with colored arrows.

FTIR and XPS analyses were conducted in order to provide information about the compositional elements and functional groups of the polyamide surface. ATR-FTIR spectra of the cross-linked asymmetric P84® support, TFC and TFNs are shown in Figure 6. The peaks at 1378 cm^{-1} and 1731 cm^{-1} in Figure 6a, marked with asterisks, correspond to the C-N and C=O bonds, respectively, of the cross-linked P84® support [22]. These peaks are substantially less intense in the TFC spectrum because the polyamide thin film had been properly formed. In consequence, new peaks that correspond to amide functionalities [22] and polyamide layer formation appear at 1639 cm^{-1} (amide I, C=O stretching vibration), 1537 cm^{-1} (amide II, C-N stretching) and 1465 cm^{-1} and 1405 cm^{-1} (amide functionalities). In the case of the ATR-FTIR spectra of the TFN membranes, the subtraction of the TFC spectrum allowed us to highlight the MOF

NPs presence, while maintaining the polyamide characteristic peaks. This indicates that the polyamide thin film was formed in the presence of MOF nanoparticles. Characteristic absorption bands of the UiO-66 are highlighted in the ATR-FTIR spectra (1398 cm^{-1} due to the stretching mode of the carboxylate group, 744 cm^{-1} to the C-H bending and 663 cm^{-1} to the Zr-μ_3-O stretching) (Figure 6b) and can be clearly seen in the TFN-UiO-66 sample, especially after the TFC subtraction. In the case of ZIF-93 samples (Figure 6c), typical peaks for ZIF-93 (1633–1658 cm^{-1}, aldehyde group) were observed in addition to other stretch bands of the ZIF-93. Regarding the ZIF-8 samples (Figure 6d), the C=N band for ZIF-8 at 1580 $cm^{-1}$is well pronounced even in the TFN-ZIF-8 sample. These findings reveal the presence of MOF NPs in all the TFN membranes.

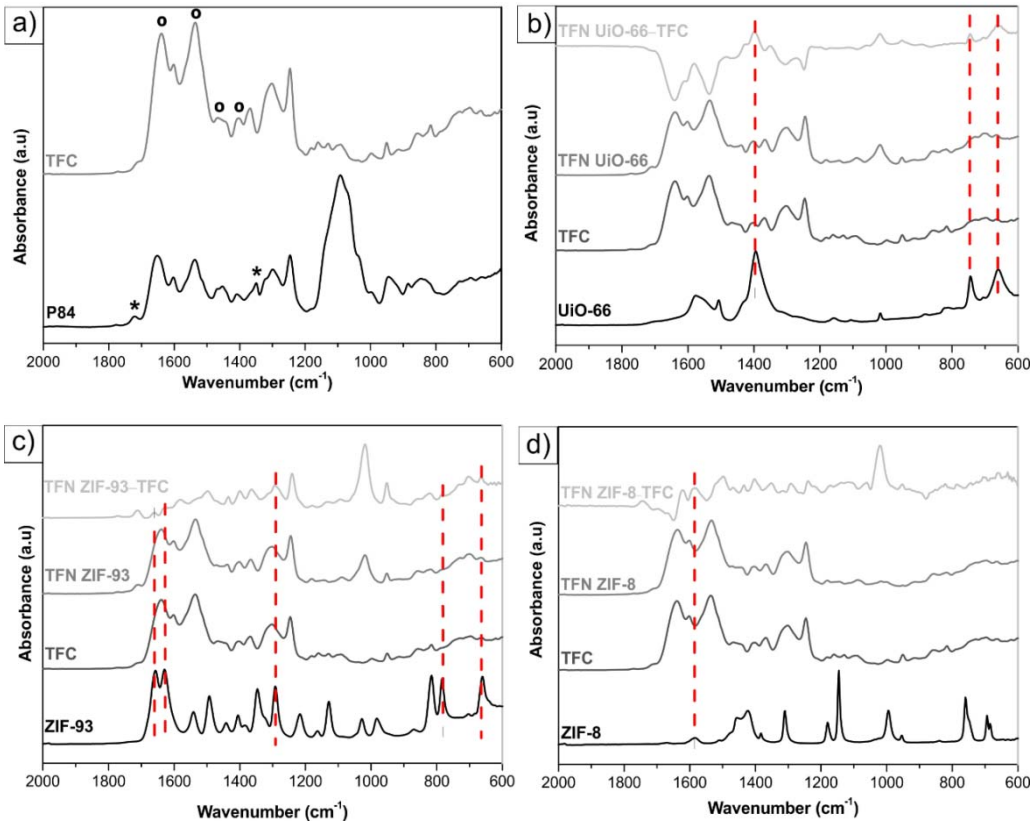

Figure 6. FTIR-ATR spectra of the MOFs synthesized in this work, cross-linked P84® support, TFC membranes, TFN membranes and TFN membranes after subtraction of the TFC membrane

spectrum**. a)** P84® and TFC membrane comparison, **b)** UiO-66 samples**, c)** ZIF-93 samples and **d)** ZIF-8 samples.

The chemical composition of the membrane surface (about 10 nm deep, where only polyamide and MOF NPs are located) was further characterized by XPS to confirm the existence of MOF NPs and quantify their abundance in the TFN membranes (Table 3). UiO-66, ZIF-93 and ZIF-8 concentrations in the top PA layer are 17.7%, 6.5% and 24.2%, respectively, being representative data of the entire membrane surface as the area of XPS analysis is 700 × 300 μm under the previously described conditions.

Moreover, when the surface of the TFN membranes was analyzed by XPS, the oxygen (O 1s), nitrogen (N 1s) and carbon (C 1s) peaks from the PA thin layer were registered. After correcting the presence of MOFs, differences in the C/N and O/N ratios were found which reflect various degrees of cross-linking of the PA layer [15]. A high degree of cross-linking in the PA layer could be a requisite to increase dye rejection [45]. It is noteworthy that the C/N and O/N ratios in the case of the TFN-ZIF-8 membrane (after subtracting element contribution from UiO-66, ZIF-93 and ZIF-8) are the highest, indicating a lower degree of cross-linking of the PA layer. The size of the ZIF-8 crystals (127 ±18 nm) may have been the reason for the existence of voids between the MOF NPs and PA layer that could have reduced the external cross-linking degree of the TFN-ZIF-8 membrane. Nonetheless, these superficial defects had no effect on the OSN performance, as will be explained in due course.

Table 3. C/N and O/N ratios, and MOF content (%) of the surface of the TFN membranes estimated from the atomic concentrations of C, N, O and metal (Zn or Zr) obtained by XPS analysis.

TFN membrane	Metal (%)[a]	C/N[b]	C/N[c]	O/N[b]	O/N[c]	MOF content (%)[d]
UiO-66	0.88	8.2	7.4	2.0	1.4	17.7
ZIF-93	0.28	7.2	7.7	1.0	1.0	6.0
ZIF-8	1.11	8.5	15.2	1.9	3.9	18.0

[a] Metal atomic concentration obtained by XPS.

[b] Element overall atomic ratio obtained directly with values from XPS.

[c] Corrected C/N and O/N ratio, excluding element concentrations from UiO-66, ZIF-93 and ZIF-8, based on chemical structure of UiO-66 ($Zr_6O_4(OH)_4(C_8\ H_4\ O_4)_6$), ZIF-93 ($ZnC_{10}H_{10}N_4O_2$), and ZIF-8 ($ZnC_8H_{12}N_4$).

[d] MOF contents were estimated from composition of metals.

Combining XPS analysis and Ar^+ ion sputtering enables an in-depth profile study to be carried out of the metal concentration and, therefore, of the distribution of MOF NPs along the PA thin film. It is important to note that because of the coexistence of different TFN components (polyamide, polyimide and MOF NPs), the number of etching cycles cannot be translated into layer thickness. Figure 7 shows the atomic percentage of Zn or Zr obtained after applying successive etching cycles from the surface of each TFN membrane until the metal composition started to decrease and the PA-PI interface presumably approached. ZIF-8 with the highest nanoparticle size (127 ±18 nm) is located mainly at the top part of the PA layer, whereas UiO-66 NPs, with a lower nanoparticle size (48 ±9 nm), goes deeper into the PA layer. TEM images (Figure 5a and 5e) indicate that UiO-66 and ZIF-8 are both well dispersed in the PA thin layer. However, the TFN-ZIF-93 membrane recorded the lowest MOF content (Table 3) and ZIF-93 NPs (67 ±13 nm) are located mainly at the surface of the PA layer. As Figure 5c

shows, ZIF-93 NPs are heterogeneously distributed and this could explain in this particular analysis the low MOF content in the surface of the TFN membrane, and within the PA layer.

Interactions between MOF (using the linker) [46] and PA can be considered in terms of Hansen solubility parameters (HSP) distance (Ra) (Table 4). The lowest Ra values calculated for MOF linker-PA layer correspond to ZIF-93 which suggests a good interaction between the PA layer and this MOF.

Table 4. Hansen solubility parameter distance (Ra) calculated as described in Hansen [47], obtained by using HSP of each solvent and PA.

	δ_D (MPa$^{0.5}$)	δ_P (MPa$^{0.5}$)	δ_H (MPa$^{0.5}$)	Ra – PA/ linker (MPa$^{0.5}$)
Polyamide (PA)	18.0	11.9	7.9	-
UiO-66 linker[a]	20.0	7.2	12.8	7.9
ZIF-93 linker[b]	18.8	10.7	9.7	2.7
ZIF-8 linker[c]	19.1	16.3	10.4	5.5

[a] Benzene-1,4-dicarboxylic acid

[b] 4-methyl-5-imidazolecarboxaldehyde

[c] 2-methylimidazole

[d] Calculated according to $Ra^2 = 4(\delta_{D1} - \delta_{D2})^2 + (\delta_{P1} - \delta_{P2})^2 + (\delta_{H1} - \delta_{H2})^2$ where δ_{D1}, δ_{P1} and δ_{H1} and δ_{D2}, δ_{P2} and δ_{H2} are sets of parameters corresponding to PA or hexane and MOF linker, respectively.

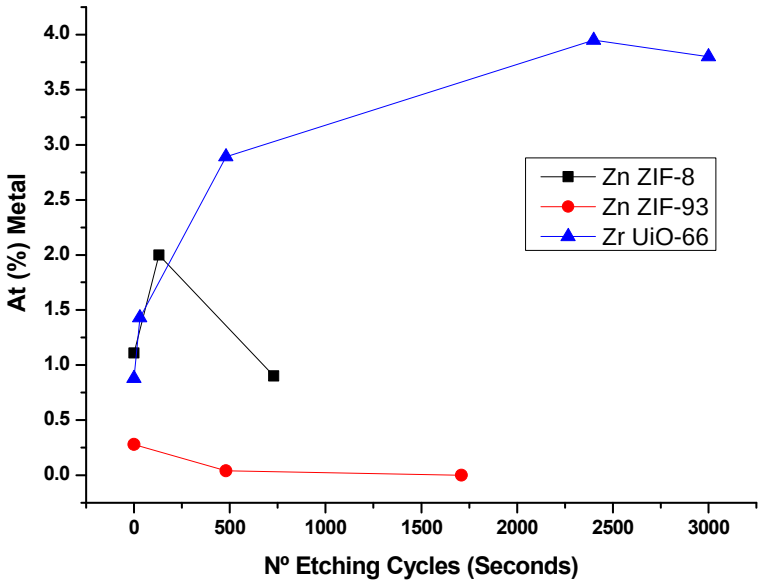

Figure 7. Atomic percentage of metal (Zn or Zr) along an in-depth profile study (etching cycles in seconds) from the surface of each TFN membrane (TFN-UiO-66, TFN-ZIF-93 and TFN-ZIF-8).

Table 2 shows the contact angle of the TFC and TFN membranes. When hydrophobic ZIF-8 is used as the filler, the contact angle slightly increases in comparison to TFC whereas if UiO-66 or ZIF-93 are added (both are hydrophilic) the contact angle decreases. This trend was also observed by Sorribas et al. [14] who prepared TFN membranes using MOFs with different hydrophilic/hydrophobic properties as fillers and saw how the membranes acquired the same character as the MOF added.

3.4. TFN membrane performance

To check the interchangeability of DMF and DMSO in the post-treatments following the preparation of TFNs, TFN membranes using ZIF-8 as a filler (which is usually used as a model MOF) were tested with both solvents obtaining the results shown in Table S2.

As an example, after post-treatment of the membrane by filtration with DMF, the permeance obtained was 6.7 $L \cdot m^{-2} \cdot h^{-1} \cdot bar^{-1}$ whereas in the case of using DMSO this permeance was 8.5 $L \cdot m^{-2} \cdot h^{-1} \cdot bar^{-1}$. As in the case of the TFC membranes, the results obtained with both solvents were similar, being slightly better when DMSO was used as the activating solvent, thus demonstrating that DMSO is a greener substitute for DMF.

After checking that both solvents are interchangeable, MOF-TFN membranes using UiO-66, ZIF-8 and ZIF-93 as fillers were activated using DMSO. Figure 8 shows the permeances and the rejections obtained before and after the DMSO filtration post-treatment. As can be seen, for all the membranes, both were higher after the filtration post-treatment. This is consistent with the findings reported in previous works [16].

On the other hand, as reported in previous works, the addition of fillers inside the thin film [14,16] increases the permeance of TFN in comparison with TFC membranes. Thanks to the small size of the MOFs, the thickness of the polyamide layer is nanometric and besides, the porosity of the MOF improves the permeances of the TFN membranes whereas the rejection is almost the same. The highest permeance is obtained when either UiO-66 or ZIF-93 is used as filler, being 11±0.7 L m^{-2} h^{-1} bar^{-1} and 11±0.6 L m^{-2} h^{-1} bar^{-1}, respectively (Table S2). In the case of UiO-66 the rejection is worse, an effect than can be explained taking into account that this MOF presents the largest pore size and also the worst interaction with PA in terms of the Hansen solubility parameters.

This would be compatible with a higher amount of microdefects in UiO-66 based TFN membranes as compared with those obtained from ZIF-8 and ZIF-93 (see table 4). In the case of ZIF-8, the permeance is improved in comparison with TFC but it is not as high as with the other fillers. As can be seen in Table 1, the addition of ZIF-8 makes the membrane more hydrophobic which favors membrane fouling and thus a decrease in the permeance [48]. Besides, the thickness, as seen by SEM (Figure 4), is greater than those corresponding to the other two MOF TFN membranes.

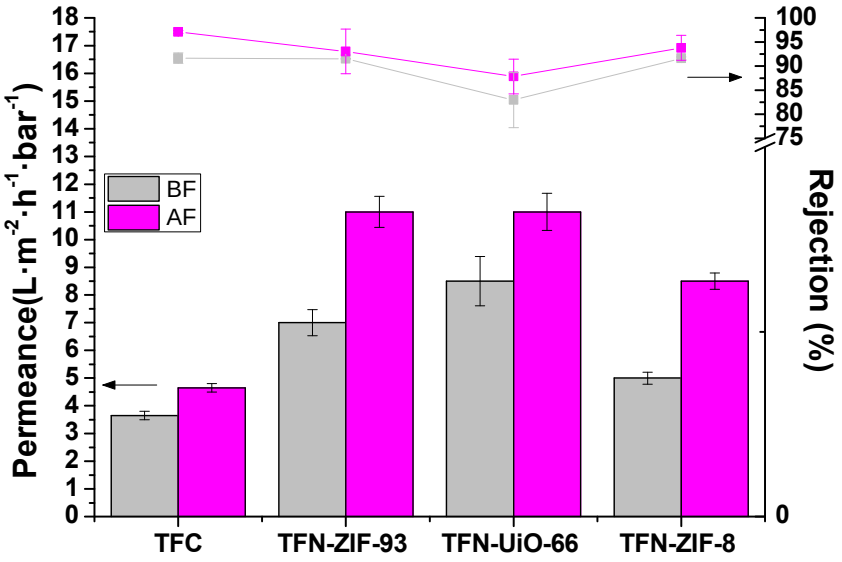

Figure 8. Performance of TFC and TFN membranes in the nanofiltration of MeOH+SY, before (BF)(grey) and after (AF) (purple) filtration post-treatment with DMSO.

Several studies have reported the fabrication of TFN membranes for OSN using different kinds of nanoparticles as fillers. Table 5 summarizes the OSN performance of different TFN membranes reported in literature. For example, Sorribas et al. [14] fabricated TFN membranes using four MOFs with different hydrophilic/hydrophobic character as filler for the nanofiltration of polystyrene oligomers in MeOH, obtaining

the highest permeance enhancement (160%) when MIL-101(Cr) was used as filler maintaining the rejection over 90%. Guo et al. [49] addedUiO-66-NH_2 into the PA layer and applied the synthesized membrane in the nanofiltration of tetracycline in methanol. They obtained a permeance enhancement of 94% and a rejection over 99%. In our work the permeance enhancements achieved are similar to those corresponding to other MOFs in the literature and there are higher permeance enhancements when carbon-based materials are used (CNT [50] and GO [51]). In any event, it should be taken in account that the comparison between them is difficult due to both the nanofiltrated solutes and the membrane polymers used are not the same.

Table 5: OSN performance of TFN membranes with different fillers.

Nanoparticle[a]	**Polymer[b]**	**Feed[c]**	**Permeance ($L \cdot m^{-2} \cdot h^{-1} \cdot bar^{-1}$)**	**Permeance enhancement[d] (%)**	**Rejection (%)**	**Ref.**
ZIF-8	P84®	PS+MeOH	2.1	40	99.5	[14]
MIL-53(Al)			1.9	27	99.9	
NH2-MIL-53(Al)			1.8	20	99.8	
MIL-101(Cr)			3.9	160	98.5	
MIL-68	P84®	SY+MeOH	4.4	16	93.8	[16]
MIL-101(Cr)			4.6	21	95	
ZIF-11			6.2	63	91.5	
UiO-66-NH_2	Matrimid®	TC+MeOH	20	94	99	[49]
Functionalized TiO_2	Matrimid®	BTB+MeOH	123.3	1	90	[11]
		CV+MeOH	124.2	0	93	
CNT	PES	BBR+MeOH	6.3	320	91	[50]
		SO+MeOH	7.2	380	71	
GO	PAN	RB+MeOH	15.3	920	98.5	[51]

Functionalized SiO_2	PAN	PEG+EtOH	3.1	72	86	[52]
ZIF-8	P84®	SY+MeOH	8.5	81	95.2	This work
ZIF-93			11	134	93.1	
UiO-66			11	134	97.9	

[a]CNT: carbon nanotubes; GO: Graphene oxide
[b]PES: polyethersulfone; PAN: polyacrylonitrile.
[c]PS: polystyrene (450 g·mol^{-1}); SY: Sunset Yellow (452 g·mol^{-1}); TC: tetracycline (444 g·mol^{-1}); BTB: bromothymol Blue (624 g·mol^{-1}); CV: Crystal Violet (408 g·mol^{-1}); BBR: Brilliant Blue R (826 g·mol^{-1}); Safranin O: (351 g·mol^{-1}); RB: Rose Bengal (1017 g·mol^{-1}); PEG: polyethylene glycol (450 g·mol^{-1})
[d]The permeance enhancement was calculated as follows: $\% = \frac{P_{TFN} - P_{TFC}}{P_{TFC}} \cdot 100$

To study the effect of a sequence of different pure solvent filtrations on the performance of the synthesized membranes, TFC, TFN-UiO-66 and TFN-ZIF-8 membranes post-treated with DMSO were submitted to 30 min of nanofiltration experiments at 20 bar of feed pressure, using first distilled water, then methanol, THF, acetone, and finally distilled water again. Two TFC membranes and one TFN membrane of each type were used for the permeance calculations.

Solvent permeances through the TFC and TFN membranes follow the same pattern: $water_{initial}$ > acetone > $water_{final}$ > methanol > THF. Nanofiltration performance thorough TFC and TFN membranes is a result of complex membrane-solvent interactions [16,53-54]. Viscosity, surface tension, permittivity, solvent-selective layer polymer (PA) interactions (estimated by HSP comparison) and the kinetic diameter of the solvent (see Table S1) are highly significant parameters in the permeance of different solvents. Due to the fact that polarity is considered a relevant parameter [53-54], THF, a non-polar solvent with good interaction with PA (see Ra value in Table S1), should have shown the highest flow. However, THF permeance is the lowest of all of them, explained by its larger kinetic diameter that is also reported as an important factor

[54]. In the same way, in general high permeance was obtained for water because of its small kinetic diameter, in spite of its high viscosity, surface tension, and especially high relative permittivity and Ra values.

Interestingly, the methanol permeance of each type of membrane did not reach the high values obtained after applying methanol and SY filtration (Table S2 and Fig. S7). Furthermore, the water permeance during the second filtration cycle was not as high as during the first cycle in any of the cases. This is probably due to the fact that the duration of the methanol experiment was not long enough to remove the water from the membrane pores (and the same happened when a new solvent is used regarding the previous solvent). Thus, higher solvent permeances would be expected in these experiments if every solvent was filtrated alone.

Acetone permeance has been reported to be the highest in similar experiments [16] because of its low relative permittivity, good interaction with PA (see Ra value in Table S1) and small kinetic diameter. In fact, if the effect of the first cycle of water filtration had not been considered, acetone permeance would have been the highest. Therefore, solvent-membrane interaction and the kinetic diameters of solvents are significant factors that cannot be ruled out, as Echaide-Gorriz et al. [16] previously reported.

As shown in Figure 9, in general permeances were higher with TFN than with TFC membranes. The effect of the presence of MOF fillers in the membranes was significant when filtering acetone, although it was also relevant when filtering THF with TFN-UiO-66 membranes. The big pores of UiO-66 boost the THF flow, as opposed to ZIF-8. Besides, when water was fed during the first cycle (when the membranes were unaltered), the permeance with UiO-66 was higher than with ZIF-8. According to Darvishmanesh et al. [53], hydrophilic membranes tend to show higher affinity and

permeances to water, and the addition of UiO-66 fillers made the thin film more hydrophilic (see contact angle measurements, Table 2). On the other hand, in the second water cycle carried out after the nanofiltration of THF, the flow was greater in the ZIF-8 due to the blockage of the THF molecules that had not been eliminated in the exchange of one solvent to another.

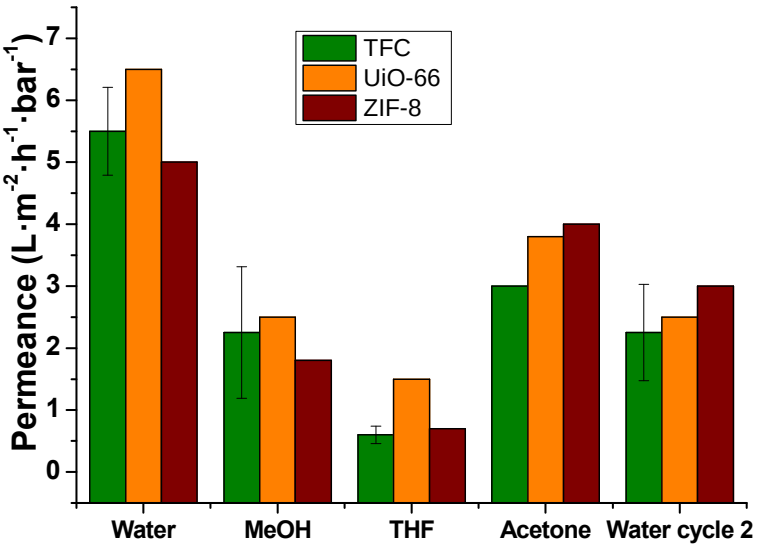

Figure 9. Effect of pure solvent in OSN using TFC (green), TFN-UiO-66 (orange) and TFN-ZIF-8 (brown) membranes after filtration post-treatment with DMSO.

4. CONCLUSIONS

The substitution of DMF as casting and activating solvent in the preparation of TFC and TFN membranes by the greener DMSO has been assessed. Characterization by SEM, AFM, contact angle and gel content of TFC membranes post-treated with both solvents revealed few differences between them. Nanofiltration of MeOH with Sunset Yellow produced similar results, these being slightly better when using DMSO owing to an increase in roughness.

The substitution of DMF by DMSO as an activating solvent was also verified on a TFN membrane containing ZIF-8. This methodology was subsequently extended to the preparation of TFNs using other MOFs: UiO-66 and ZIF-93. This is the first time that ZIF-93 has been employed for a TFN membrane. The presence and maintenance of the crystal structure of the different MOFs in the TFN membrane was confirmed by a battery of characterization techniques that include XPS, FTIR and electron diffraction. In addition, the TFN membranes were characterized by SEM showing a PA layer in which the MOF was embedded, a contact angle that depends on the hydrophilicity/hydrophobicity of the MOF, and the Hansen solubility parameters that predict the MOF/polymer interactions.

The results of methanol nanofiltration with sunset yellow reveal that the performance may be due to a combination of several factors such as the porosity of the MOF, polyamide-MOF layer thickness and the hydrophilic/hydrophobic character of the membrane. When UiO-66, which has the highest pore size but worse interaction with PA, was used as a filler, a value of 11 $L \cdot m^{-2} \cdot h^{-1} \cdot bar^{-1}$ of methanol (2.3 times higher than TFC membrane) was obtained with a rejection of 88%. When ZIF-93, which has better interaction with PA, was used as a filler, a similar value of 11 $L \cdot m^{-2} \cdot h^{-1} \cdot bar^{-1}$ was obtained improving the rejection up to 93%. Comparing the permeation of different pure solvents through a TFN membrane under the conditions studied shows that the pore sizes of the MOF and the size of the solvent are the most important factors.

ACKNOWLEDGMENT

Financial support from the Spanish MINECO and FEDER (MAT2016-77290-R), the Aragón Government (T43-17R) and the ESF is gratefully acknowledged. L. P. thanks the Spanish Ministry of Economy, Industry and Competitiveness Program FPI2014 for her PhD grant. All the microscopy work was done in the Laboratorio de Microscopías

Avanzadas at the Instituto de Nanociencia de Aragón (LMA-INA). Finally, the authors would like to acknowledge the use of the Servicio General de Apoyo a la Investigación-SAI, Universidad de Zaragoza. Prof. Dr Steven Abbott is thanked for providing Hansen solubility parameters.

APPENDIX A. SUPPLEMENTARY DATA

REFERENCES

[1] Marchetti, P.; Solomon, M. F. J.; Szekely, G.; Livingston, A. G., Molecular Separation with Organic Solvent Nanofiltration: A Critical Review. *Chemical Reviews,* 21 (2014) 10735-10806.
[2] Radjenović, J.; Petrović, M.; Ventura, F.; Barceló, D., Rejection of pharmaceuticals in nanofiltration and reverse osmosis membrane drinking water treatment. *Water Research,* 14 (2008) 3601-3610.
[3] Košutić, K.; Furač, L.; Sipos, L.; Kunst, B., Removal of arsenic and pesticides from drinking water by nanofiltration membranes. *Separation and Purification Technology,* 2 (2005) 137-144.
[4] Tang, C.; Chen, V., Nanofiltration of textile wastewater for water reuse. *Desalination,* 1 (2002) 11-20.
[5] Buonomenna, M. G.; Bae, J., Organic Solvent Nanofiltration in Pharmaceutical Industry. *Sep. Purif. Rev.,* 2 (2015) 157-182.
[6] Petersen, R. J., Composite reverse osmosis and nanofiltration membranes. *J. Membr. Sci.,* 1 (1993) 81-150.
[7] Jeong, B.-H.; Hoek, E. M. V.; Yan, Y.; Subramani, A.; Huang, X.; Hurwitz, G.; Ghosh, A. K.; Jawor, A., Interfacial polymerization of thin film nanocomposites: A new concept for reverse osmosis membranes. *J. Membr. Sci.,* 1–2 (2007) 1-7.
[8] Lau, W. J.; Gray, S.; Matsuura, T.; Emadzadeh, D.; Paul Chen, J.; Ismail, A. F., A review on polyamide thin film nanocomposite (TFN) membranes: History, applications, challenges and approaches. *Water Res.,* Supplement C (2015) 306-324.
[9] Emadzadeh, D.; Lau, W. J.; Matsuura, T.; Rahbari-Sisakht, M.; Ismail, A. F., A novel thin film composite forward osmosis membrane prepared from PSf–TiO2 nanocomposite substrate for water desalination. *Chem. Eng. J. (Lausanne),* (2014) 70-80.
[10] Soroko, I.; Livingston, A., Impact of TiO2 nanoparticles on morphology and performance of crosslinked polyimide organic solvent nanofiltration (OSN) membranes. *J. Membr. Sci.,* 1 (2009) 189-198.
[11] Peyravi, M.; Jahanshahi, M.; Rahimpour, A.; Javadi, A.; Hajavi, S., Novel thin film nanocomposite membranes incorporated with functionalized TiO2 nanoparticles for organic solvent nanofiltration. *Chem. Eng. J. (Lausanne),* (2014) 155-166.
[12] Yin, J.; Kim, E.-S.; Yang, J.; Deng, B., Fabrication of a novel thin-film nanocomposite (TFN) membrane containing MCM-41 silica nanoparticles (NPs) for water purification. *J. Membr. Sci.,* (2012) 238-246.
[13] Yin, J.; Zhu, G.; Deng, B., Graphene oxide (GO) enhanced polyamide (PA) thin-film nanocomposite (TFN) membrane for water purification. *Desalination,* (2016) 93-101.
[14] Sorribas, S.; Gorgojo, P.; Téllez, C.; Coronas, J.; Livingston, A. G., High Flux Thin Film Nanocomposite Membranes Based on Metal–Organic Frameworks for Organic Solvent Nanofiltration. *J. Am. Chem. Soc.,* 40 (2013) 15201-15208.
[15] Duan, J.; Pan, Y.; Pacheco, F.; Litwiller, E.; Lai, Z.; Pinnau, I., High-performance polyamide thin-film-nanocomposite reverse osmosis membranes containing hydrophobic zeolitic imidazolate framework-8. *J. Membr. Sci.,* (2015) 303-310.

[16] Echaide-Gorriz, C.; Sorribas, S.; Tellez, C.; Coronas, J., MOF nanoparticles of MIL-68(Al), MIL-101(Cr) and ZIF-11 for thin film nanocomposite organic solvent nanofiltration membranes. *RSC Adv.,* 93 (2016) 90417-90426.
[17] Wang, H.; Zeng, Z.; Xu, P.; Li, L.; Zeng, G.; Xiao, R.; Tang, Z.; Huang, D.; Tang, L.; Lai, C.; Jiang, D.; Liu, Y.; Yi, H.; Qin, L.; Ye, S.; Ren, X.; Tang, W., Recent progress in covalent organic framework thin films: fabrications, applications and perspectives. *Chem. Soc. Rev.,* 2 (2019) 488-516.
[18] Jiang, D.; Xu, P.; Wang, H.; Zeng, G.; Huang, D.; Chen, M.; Lai, C.; Zhang, C.; Wan, J.; Xue, W., Strategies to improve metal organic frameworks photocatalyst's performance for degradation of organic pollutants. *Coord. Chem. Rev.,* (2018) 449-466.
[19] Xiong, W.; Zeng, Z.; Li, X.; Zeng, G.; Xiao, R.; Yang, Z.; Zhou, Y.; Zhang, C.; Cheng, M.; Hu, L.; Zhou, C.; Qin, L.; Xu, R.; Zhang, Y., Multi-walled carbon nanotube/amino-functionalized MIL-53(Fe) composites: Remarkable adsorptive removal of antibiotics from aqueous solutions. *Chemosphere,* (2018) 1061-1069.
[20] Guillen, G. R.; Pan, Y.; Li, M.; Hoek, E. M. V., Preparation and Characterization of Membranes Formed by Nonsolvent Induced Phase Separation: A Review. *Ind. Eng. Chem. Res.,* 7 (2011) 3798-3817.
[21] Echaide-Gorriz, C.; Navarro, M.; Ariso, C. T.; Coronas, J., Simultaneous use of MOFs MIL-101 (Cr) and ZIF-11 for Thin Film Nanocomposite Organic Solvent Nanofiltration. *Dalton Transactions,* (2017) 6244-6252.
[22] Jimenez Solomon, M. F.; Bhole, Y.; Livingston, A. G., High flux membranes for organic solvent nanofiltration (OSN)—Interfacial polymerization with solvent activation. *J. Membr. Sci.,* (2012) 371-382.
[23] EPA US EPA website. https://www.epa.gov/greeenchemistry.
[24] Anastas, P. T.; Kirchhoff, M. M., Origins, current status, and future challenges of green chemistry. *Accounts of Chemical Research,* (2002) 686-694.
[25] Prat, D.; Pardigon, O.; Flemming, H.-W.; Letestu, S.; Ducandas, V. r.; Isnard, P.; Guntrum, E.; Senac, T.; Ruisseau, S. p.; Cruciani, P., Sanofi's solvent selection guide: a step toward more sustainable processes. *Organic Process Research & Development,* 12 (2013) 1517-1525.
[26] ECHA Candidate List of substances of very high concern for Authorisation. https://echa.europa.eu/candidate-list-table.
[27] Burgal, J. D.; Peeva, L.; Livingston, A., Towards improved membrane production: using low-toxicity solvents for the preparation of PEEK nanofiltration membranes. *Green Chemistry,* 8 (2016) 2374-2384.
[28] Hua, D.; Japip, S.; Wang, K. Y.; Chung, T.-S., Green Design of Poly(m-Phenylene Isophthalamide)-Based Thin-Film Composite Membranes for Organic Solvent Nanofiltration and Concentrating Lecithin in Hexane. *ACS Sustain. Chem. Eng.,* 8 (2018) 10696-10705.
[29] Figoli, A.; Marino, T.; Simone, S.; Di Nicolo, E.; Li, X.-M.; He, T.; Tornaghi, S.; Drioli, E., Towards non-toxic solvents for membrane preparation: a review. *Green Chemistry,* 9 (2014) 4034-4059.
[30] Soroko, I.; Bhole, Y.; Livingston, A. G., Environmentally friendly route for the preparation of solvent resistant polyimide nanofiltration membranes. *Green Chem.,* 1 (2011) 162-168.
[31] Capello, C.; Fischer, U.; Hungerbuhler, K., What is a green solvent? A comprehensive framework for the environmental assessment of solvents. *Green Chem.,* 9 (2007) 927-934.
[32] Valenzano, L.; Civalleri, B.; Chavan, S.; Bordiga, S.; Nilsen, M. H.; Jakobsen, S.; Lillerud, K. P.; Lamberti, C., Disclosing the Complex Structure of UiO-66 Metal Organic Framework: A Synergic Combination of Experiment and Theory. *Chemistry of Materials,* 7 (2011) 1700-1718.
[33] Morris, W.; He, N.; Ray, K. G.; Klonowski, P.; Furukawa, H.; Daniels, I. N.; Houndonougbo, Y. A.; Asta, M.; Yaghi, O. M.; Laird, B. B., A Combined Experimental-Computational Study on the Effect of Topology on Carbon Dioxide Adsorption in Zeolitic Imidazolate Frameworks. *J. Phys. Chem. C,* 45 (2012) 24084-24090.

[34] Park, K. S.; Ni, Z.; Cote, A. P.; Choi, J. Y.; Huang, R. D.; Uribe-Romo, F. J.; Chae, H. K.; O'Keeffe, M.; Yaghi, O. M., Exceptional chemical and thermal stability of zeolitic imidazolate frameworks. *Proceedings of the National Academy of Sciences of the United States of America,* (2006) 10186-10191.
[35] Liu, X.; Li, Y.; Ban, Y.; Peng, Y.; Jin, H.; Bux, H.; Xu, L.; Caro, J.; Yang, W., Improvement of hydrothermal stability of zeolitic imidazolate frameworks. *Chem. Commun. (Cambridge, U. K.),* 80 (2013) 9140-9142.
[36] Liédana, N.; Galve, A.; Rubio, C.; Téllez, C.; Coronas, J., CAF@ZIF-8: One-Step Encapsulation of Caffeine in MOF. *ACS Appl. Mater. Interfaces,* 9 (2012) 5016-5021.
[37] Hou, L.; Wang, L.; Zhang, N.; Xie, Z.; Dong, D., Polymer brushes on metal-organic frameworks by UV-induced photopolymerization. *Polym. Chem.,* 37 (2016) 5828-5834.
[38] Yang, Q.; Wiersum, A. D.; Jobic, H.; Guillerm, V.; Serre, C.; Llewellyn, P. L.; Maurin, G., Understanding the Thermodynamic and Kinetic Behavior of the CO2/CH4 Gas Mixture within the Porous Zirconium Terephthalate UiO-66(Zr): A Joint Experimental and Modeling Approach. *J. Phys. Chem. C,* 28 (2011) 13768-13774.
[39] Sorribas, S.; Zornoza, B.; Tellez, C.; Coronas, J., Ordered mesoporous silica-(ZIF-8) core-shell spheres. *Chem. Commun. (Cambridge, U. K.),* 75 (2012) 9388-9390.
[40] Cavka, J. H.; Jakobsen, S.; Olsbye, U.; Guillou, N.; Lamberti, C.; Bordiga, S.; Lillerud, K. P., A New Zirconium Inorganic Building Brick Forming Metal Organic Frameworks with Exceptional Stability. *J. Am. Chem. Soc.,* 42 (2008) 13850-13851.
[41] Chavan, S.; Vitillo, J. G.; Gianolio, D.; Zavorotynska, O.; Civalleri, B.; Jakobsen, S.; Nilsen, M. H.; Valenzano, L.; Lamberti, C.; Lillerud, K. P.; Bordiga, S., H_2 storage in isostructural UiO-67 and UiO-66 MOFs. *Phys. Chem. Chem. Phys.,* 5 (2012) 1614-1626.
[42] Gupta, K. M.; Qiao, Z.; Zhang, K.; Jiang, J., Seawater Pervaporation through Zeolitic Imidazolate Framework Membranes: Atomistic Simulation Study. *ACS Appl. Mater. Interfaces,* 21 (2016) 13392-13399.
[43] Gorgojo, P.; Jimenez-Solomon, M.; Livingston, A., Polyamide thin film composite membranes on cross-linked polyimide supports: Improvement of RO performance via activating solvent. *Desalination,* (2014) 181-188.
[44] Sánchez-Laínez, J.; Paseta, L.; Navarro, M.; Zornoza, B.; Téllez, C.; Coronas, J., Ultrapermeable Thin Film ZIF-8/Polyamide Membrane for H2/CO2 Separation at High Temperature without Using Sweep Gas. *Adv. Mater. Interfaces,* 19 (2018) 1800647.
[45] Ghosh, A. K.; Jeong, B.-H.; Huang, X.; Hoek, E. M. V., Impacts of reaction and curing conditions on polyamide composite reverse osmosis membrane properties. *J. Membr. Sci.,* 1 (2008) 34-45.
[46] Paseta, L.; Potier, G.; Abbott, S.; Coronas, J., Using Hansen solubility parameters to study the encapsulation of caffeine in MOFs. *Org. Biomol. Chem.,* 6 (2015) 1724-1731.
[47] Hansen, C. M., 50 Years with solubility parameters—past and future. *Prog. Org. Coat.,* 1 (2004) 77-84.
[48] Koo, C. H.; Mohammad, A. W.; Suja', F.; Meor Talib, M. Z., Review of the effect of selected physicochemical factors on membrane fouling propensity based on fouling indices. *Desalination,* (2012) 167-177.
[49] Guo, X.; Liu, D.; Han, T.; Huang, H.; Yang, Q.; Zhong, C., Preparation of thin film nanocomposite membranes with surface modified MOF for high flux organic solvent nanofiltration. *AIChE J.,* 4 (2017) 1303-1312.
[50] Roy, S.; Ntim, S. A.; Mitra, S.; Sirkar, K. K., Facile fabrication of superior nanofiltration membranes from interfacially polymerized CNT-polymer composites. *J. Membr. Sci.,* 1 (2011) 81-87.
[51] Shao, L.; Cheng, X.; Wang, Z.; Ma, J.; Guo, Z., Tuning the performance of polypyrrole-based solvent-resistant composite nanofiltration membranes by optimizing polymerization conditions and incorporating graphene oxide. *J. Membr. Sci.,* (2014) 82-89.

[52] Li, Y.; Mao, H.; Zhang, H.; Yang, G.; Ding, R.; Wang, J., Tuning the microstructure and permeation property of thin film nanocomposite membrane by functionalized inorganic nanospheres for solvent resistant nanofiltration. *Sep. Purif. Technol.,* (2016) 60-70.
[53] Darvishmanesh, S.; Buekenhoudt, A.; Degrève, J.; Van der Bruggen, B., General model for prediction of solvent permeation through organic and inorganic solvent resistant nanofiltration membranes. *J. Membr. Sci.,* 1 (2009) 43-49.
[54] Siavash, D.; Jan, D.; Bart, V. d. B., Physicochemical Characterization of Transport in Nanosized Membrane Structures. *ChemPhysChem,* 2 (2010) 404-411.

Figure captions

Figure 1. a) Building blocks of UiO-66 with the Zr6O4(OH)4 clusters in green and chemical structure of the terephthalic acid, **b)** Building blocks of ZIF-93 with the ZnN4 tetrahedra in green and chemical structure of the 4-methyl-5-imidazolecarboxaldehyde linker and **c)** Building blocks of ZIF-8 with the ZnN4 tetrahedra in green and chemical structure of the 2-methylimidazole linker. Oxygen, nitrogen and carbon atoms are in red, blue and black, respectively. These structures were made with Diamond 3.2 using the corresponding CIF files [32-34]. **d, e, f)** TEM images of **d)** UiO-66, **e)** ZIF-93 and **f)** ZIF-8.

Figure 2. 3D **(a, c)** and 2D **(b, d)** AFM images of the surface of TFC membranes with a DMF **(a, b)** or DMSO **(c, d)** bath post-treatment and **e)** R_a, *RMS* and gel content values.

Figure 3. a-c) Surface SEM micrographs and **d-f)** cross-section SEM micrographs of the TFN membranes: **a)** and **d)** TFN-ZIF-93; **b)** and **e)** TFN-UiO-66; **c)** and **f)** TFN-ZIF-8.

Figure 4. SEM images of the PA+MOF layer for the MOF. **a)** ZIF-8; **b)** ZIF-93 and **c)** UiO-66.

Figure 5. a, c, e) TEM images of the PA thin film with the MOFs embedded and **b, d, f)** Electron diffraction patterns of the MOFs from the previous images, indexed according to the crystal structure of: **a, b)** ZIF-8;[34] **c, d)** ZIF-93[33] and **e, f)** UiO-66 [32]. The planes observed correspond to the MOF structure in each case. The diffraction spots are pointed with colored arrows.

Figure 6. FTIR-ATR spectra of the MOFs synthesized in this work, cross-linked P84® support, TFC membranes, TFN membranes and TFN membranes after subtraction of the TFC membrane spectrum**. a)** P84® and TFC membrane comparison, **b)** UiO-66 samples**, c)** ZIF-93 samples and **d)** ZIF-8 samples.

Figure 7. Atomic percentage of metal (Zn or Zr) along an in-depth profile study (etching cycles in seconds) from the surface of each TFN membrane (TFN-UiO-66, TFN-ZIF-93 and TFN-ZIF-8).

Figure 8. Performance of TFC and TFN membranes in the nanofiltration of MeOH+SY, before (BF)(grey) and after (AF) (purple) filtration post-treatment with DMSO.

Figure 9. Effect of pure solvent in OSN using TFC (green), TFN-UiO-66 (orange) and TFN-ZIF-8 (brown) membranes after bath and filtration post-treatment with DMSO.

Supporting Information

Greener Processes in the Preparation of Thin Film Nanocomposite Membranes with Diverse Metal-Organic Frameworks for Organic Solvent Nanofiltration

Lorena Paseta[a], *Marta Navarro*[a], *Joaquín Coronas*[a,b], *Carlos Téllez*[a,b,*]

[a]Instituto de Nanociencia de Aragón (INA) and Chemical and Environmental Engineering Department, Universidad de Zaragoza, 50018 Zaragoza, Spain.

[b]Instituto de Ciencia de Materiales de Aragón (ICMA), CSIC-Universidad de Zaragoza, 50018 Zaragoza, Spain

[*]Corresponding author: ctellez@unizar.es

MOFs SYNTHESIS

The synthesis of ZIF-93 was carried out as previously reported.[1] 0.882 g of zinc nitrate hexahydrate ($Zn(NO_3)_2 \cdot 6H_2O$ - reagent grade, Scharlau) was dissolved in 60 mL of methanol (MeOH - HPLC grade, Scharlab). Separately, 2.610 g of 4-methyl-5-imidazolecarboxaldehyde ($C_5H_6N_2O$ - 99%, Sigma-Aldrich) was dissolved in 60 mL of MeOH. The metal solution was added to the ligand solution and the mixture was stirred for 20 min at room temperature. Finally, the MOF nanoparticles were recovered, rinsed

in ethanol (EtOH - anhydrous ethanol, Prolabo) three times in cycles of centrifugation and ultrasonication and dried at room temperature.

ZIF-8 was synthesized following the same procedure as described by Liédana et al.[2] A solution of 0.95 g of $Zn(NO_3)_2 \cdot 6H_2O$ in a mixture of 20mL of methanol and 20 mL of deionized water was poured over a solution of 3.09 g of 2-methylimidazole ($C_4H_6N_2$- 99% purity, Sigma-Aldrich) in 20mL of MeOH. The final solution was stirred for two hour at room temperature. ZIF-8 nanoparticles were then separated by centrifugation, washed with ethanol and dried at room temperature.

UIO-66 nanoparticles were synthesised as previously reported.[3] First, 0.4 g of zirconium chloride ($ZrCl_4$ - >95%, Sigma Aldrich) was dissolved in 100 mL of DMF (99.5%, Scharlab) by ultrasonication at room temperature. Then, 0.28 g of terephthalic acid (C_6H_4-1,4-$(CO_2H)_2$ - 98%, Sigma Aldrich) and 0.13 mL of H_2O was added sequentially. When everything was well dissolved, the solution was transferred into an autoclave and heated at 120 °C for 24 h. The solid was then recovered and washed for three cycles of centrifugation and ultrasonication in DMF and one time with MeOH (?). Finally, the UiO-66 nanoparticles were activated in a furnace at 300 °C for 3 h, with a heating rate of 15 $°C \cdot min^{-1}$.

MOFs CHARACTERIZATION

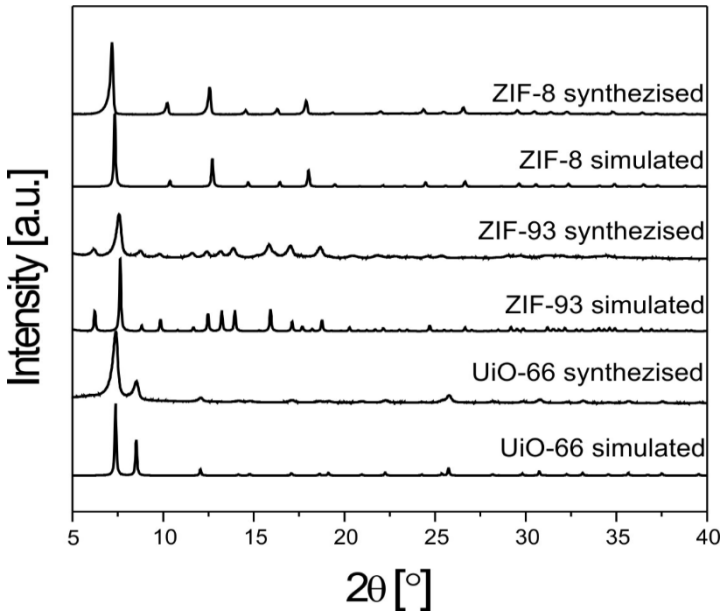

Figure S1: XRD patterns of UiO-66, ZIF-93 and ZIF-8 nanoparticles synthesized in this work compared with the simulated patterns. The simulated patterns were obtained using the corresponding CIF files.[4]

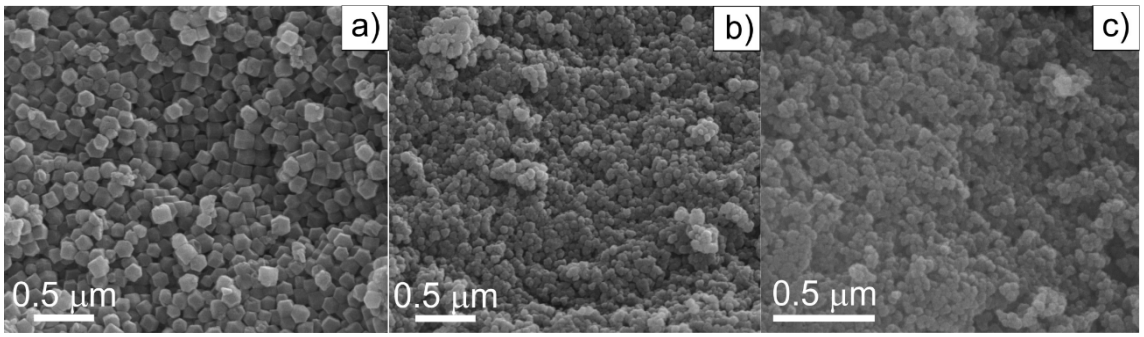

Figure S2: SEM images of MOF nanoparticles: **a)** ZIF-8; **b)** ZIF-93 and **c)** UiO-66.

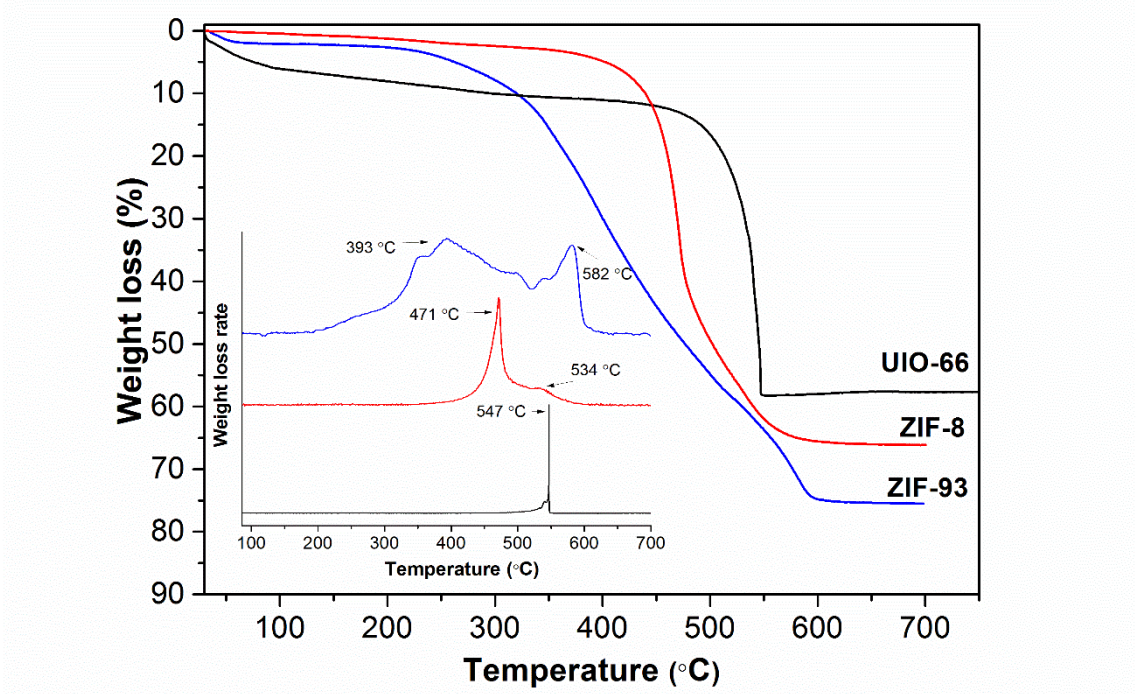

Figure S3: Weight loss curves and weight loss rate in air atmosphere of UiO-66, ZIF-93 and ZIF-8 nanoparticles at a heating rate of 10 °C·min^{-1}.

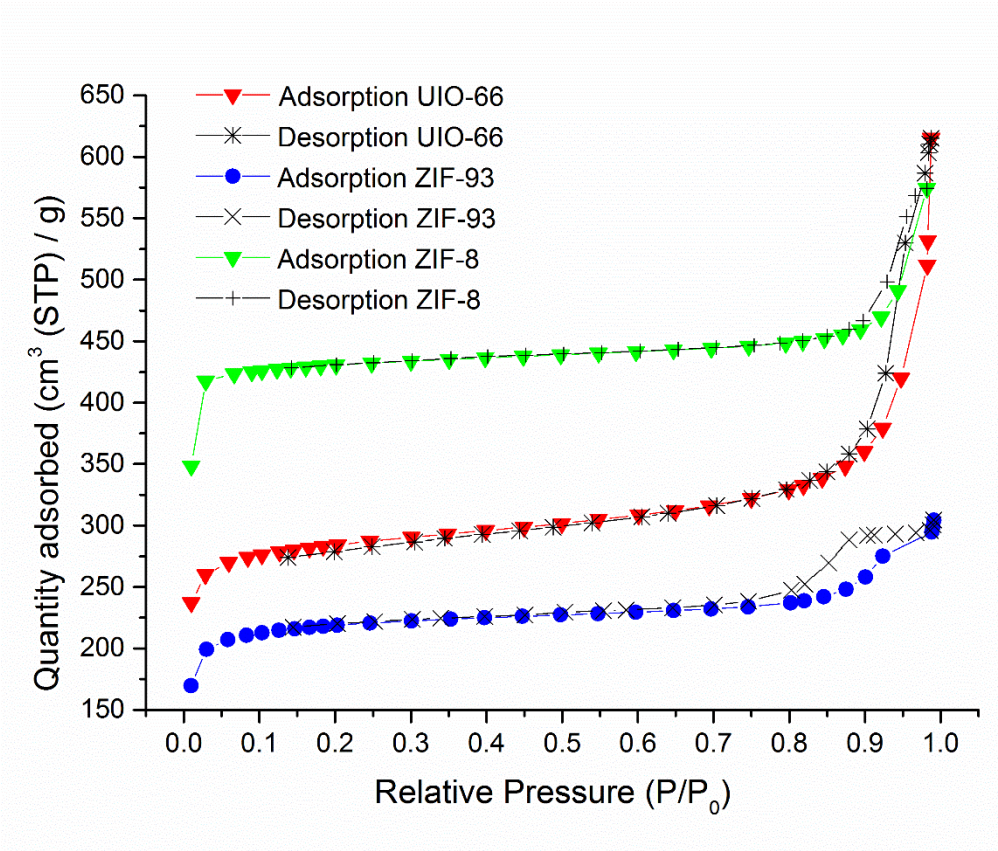

Figure S4: N_2 adsorption – desorption isotherms of the synthesized MOF nanoparticles.

MEMBRANE CHARACTERIZATION

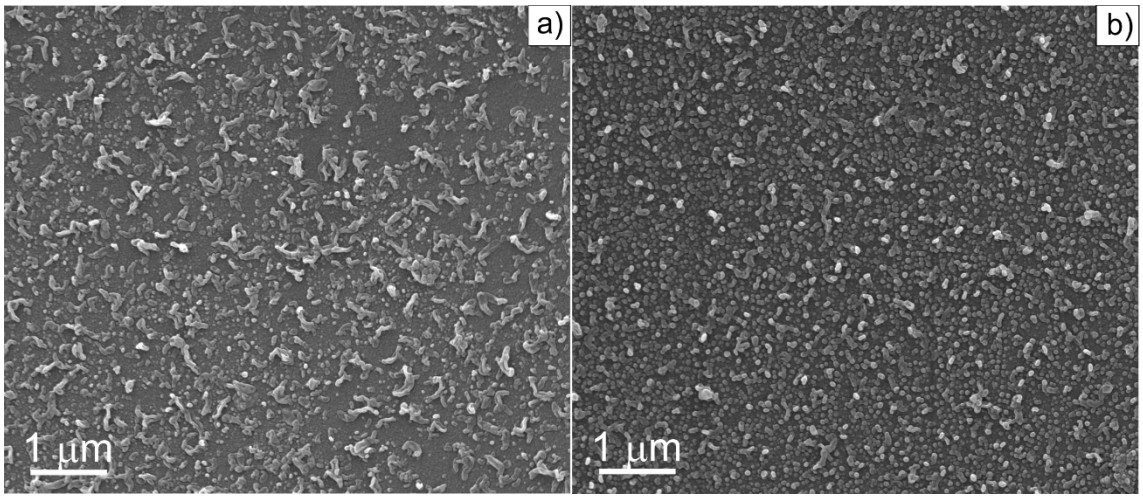

Figure S5: SEM of the surface of the TFC membranes post-treated using **a)** DMF as activating solvent; **b)** DMSO as activating solvent.

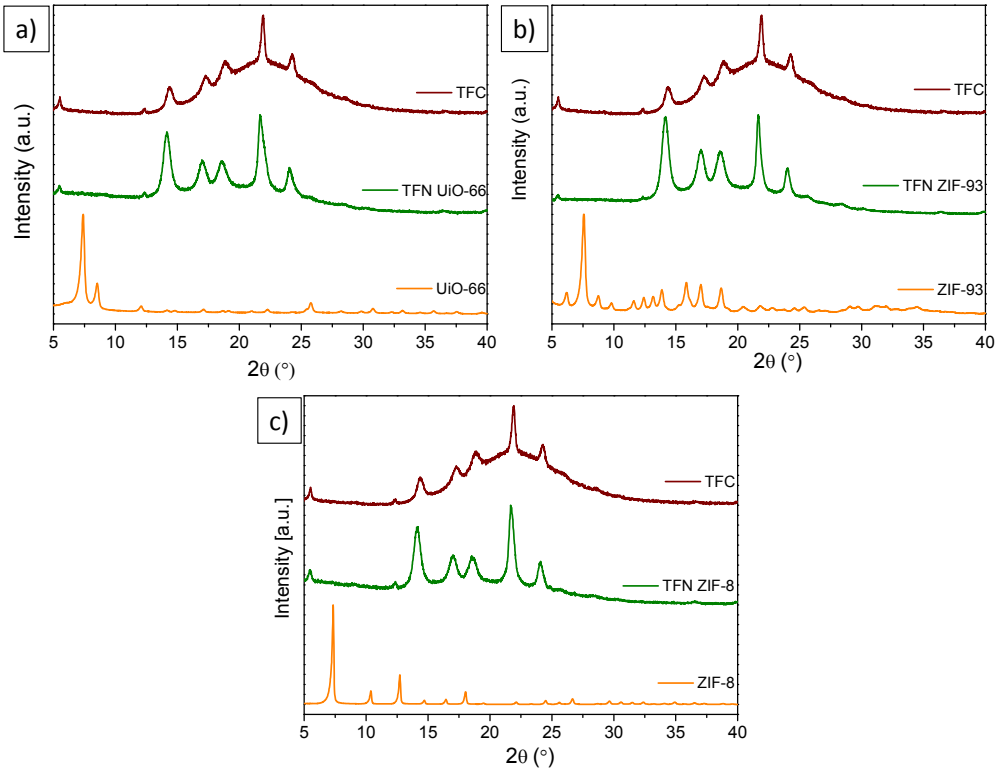

Figure S6: XRD patterns of MOF, TFN and TFC. **a)** UiO-66, **b)** ZIF-93 and **c)** ZIF-8.

MEMBRANE PERFORMANCE

Table S1: Relative permittivity, related to molecule polarity. Hansen parameter differences (Ra) calculated as described in Hansen,[5] obtained by using HSP of each solvent and either PA or P84. μ: viscosity; ϒ: surface tension; ε: relative permittivity.

	Hansen parameters								
Solvent	δ_D	δ_p	δ_H	***Ra - solvent/PI***	***Ra- solvent/PA***	**μ (cP)[6]**	**ϒ (mN/m)[6a, 6b, 7]**	**ε[8]**	**Kinetic diameter (Å)[9]**
H_2O	15.5	16.0	42.3	34.6	35.0	0.9	72.8	78.4	2.7
MeOH	14.7	12.3	22.3	15.4	15.8	0.5	22.1	33.0	3.6
THF	16.8	5.7	8.0	7.7	6.6	0.5	25.0	7.5	6.3
Acetone	15.5	10.4	7.0	5.0	5.3	0.3	23.3	21.0	4.6
DMSO	18.4	16.4	10.2	4.2	5.1	1.9	42.9	47.2	5
DMF	17.4	13.7	11.3	3.3	4.0	0.9	34.4	38.2	5.5
P84	17.5	13.3	8.0						
PA	18.0	11.9	7.9						

Table S2: Permeances and rejections before (BF) and after (AF) the filtration post-treatment. Nanofiltration conditions: 20 bar and 23 °C.

	Permeance ($L \cdot m^{-2} \cdot h^{-1} \cdot bar^{-1}$)		Rejection (%)	
	BF	**AF**	**BF**	**AF**
TFC DMF	2.5 ± 0.5	4.4 ± 1.1	91.3±4.5	97.0±3.0
TFC DMSO	3.7 ± 0.2	4.7 ± 0.2	91.7±1.1	97.1±0.3
TFN ZIF-93	7.0±0.5	11.0±0.6	91.5±0.1	93.1±4.6
TFN UiO-66	8.5±0.9	11.0±0.7	83±5.7	87.9±3.6
TFN ZIF-8	5.0±0.2	8.5±0.3	91.6±0.3	93.8±2.6
TFN ZIF-8 DMF	4.1±0.3	6.7±0.9	94.7±1.7	95.2±3.2

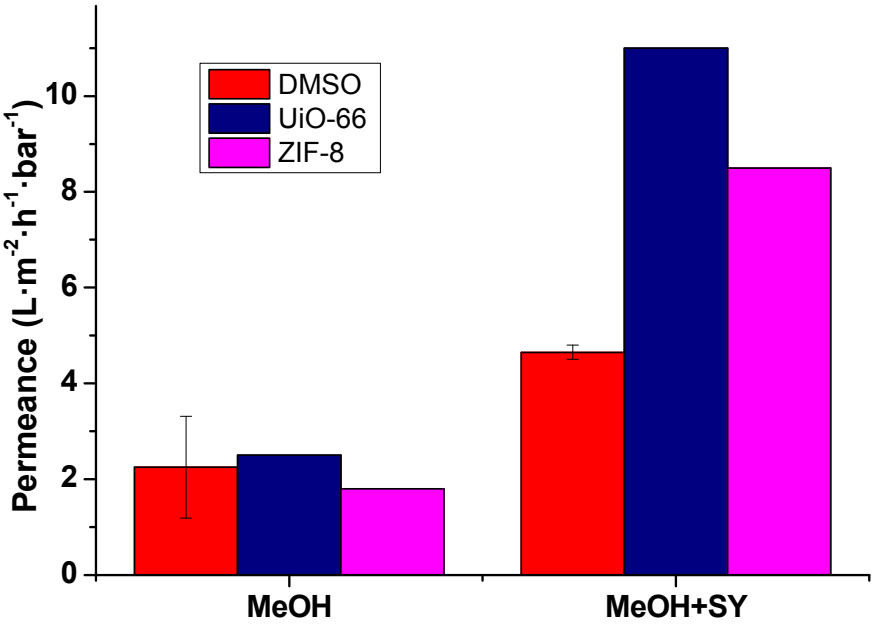

Figure S7: Permeances of pure methanol after water filtration and in the OSN of methanol-dye solution.

REFERENCES

1. Liu, X.; Li, Y.; Ban, Y.; Peng, Y.; Jin, H.; Bux, H.; Xu, L.; Caro, J.; Yang, W., Improvement of hydrothermal stability of zeolitic imidazolate frameworks. *Chem. Commun. (Cambridge, U. K.)* **2013,** *49* (80), 9140-9142.
2. Liédana, N.; Galve, A.; Rubio, C.; Téllez, C.; Coronas, J., CAF@ZIF-8: One-Step Encapsulation of Caffeine in MOF. *ACS Appl. Mater. Interfaces* **2012,** *4* (9), 5016-5021.
3. Hou, L.; Wang, L.; Zhang, N.; Xie, Z.; Dong, D., Polymer brushes on metal-organic frameworks by UV-induced photopolymerization. *Polym. Chem.* **2016,** *7* (37), 5828-5834.
4. (a) Valenzano, L.; Civalleri, B.; Chavan, S.; Bordiga, S.; Nilsen, M. H.; Jakobsen, S.; Lillerud, K. P.; Lamberti, C., Disclosing the Complex Structure of UiO-66 Metal Organic Framework: A Synergic Combination of Experiment and Theory. *Chem. Mater.* **2011,** *23* (7), 1700-1718; (b) Morris, W.; Leung, B.; Furukawa, H.; Yaghi, O. K.; He, N.; Hayashi, H.; Houndonougbo, Y.; Asta, M.; Laird, B. B.; Yaghi, O. M., A Combined Experimental−Computational Investigation of Carbon Dioxide Capture in a Series of Isoreticular Zeolitic Imidazolate Frameworks. *J. Am. Chem. Soc.* **2010,** *132* (32), 11006-11008; (c) Park, K. S.; Ni, Z.; Côté, A. P.; Choi, J. Y.; Huang, R.; Uribe-Romo, F. J.; Chae, H. K.; O'Keeffe, M.; Yaghi, O. M., Exceptional chemical and thermal stability of zeolitic imidazolate frameworks. *Proceedings of the National Academy of Sciences* **2006,** *103* (27), 10186-10191.
5. (a) Hansen, C. M., 50 Years with solubility parameters—past and future. *Prog. Org. Coat.* **2004,** *51* (1), 77-84; (b) Paseta, L.; Potier, G.; Abbott, S.; Coronas, J., Using Hansen solubility parameters to study the encapsulation of caffeine in MOFs. *Org. Biomol. Chem.* **2015,** *13* (6), 1724-1731.
6. (a) Darvishmanesh, S.; Buekenhoudt, A.; Degrève, J.; Van der Bruggen, B., General model for prediction of solvent permeation through organic and inorganic solvent resistant nanofiltration membranes. *J. Membr. Sci.* **2009,** *334* (1), 43-49; (b) Siavash, D.; Jan, D.; Bart, V. d. B., Physicochemical Characterization of Transport in Nanosized Membrane Structures. *ChemPhysChem* **2010,** *11* (2), 404-411; (c) Yang, X. J.; Livingston, A. G.; Freitas dos Santos, L., Experimental observations of nanofiltration with organic solvents. *J. Membr. Sci.* **2001,** *190* (1), 45-55; (d) Aminabhavi, T. M.; Gopalakrishna, B., Density, Viscosity, Refractive Index, and Speed of Sound in Aqueous Mixtures of N,N-Dimethylformamide, Dimethyl Sulfoxide, N,N-Dimethylacetamide, Acetonitrile, Ethylene Glycol, Diethylene Glycol, 1,4-Dioxane, Tetrahydrofuran, 2-Methoxyethanol, and 2-Ethoxyethanol at 298.15 K. *J. Chem. Eng. Data* **1995,** *40* (4), 856-861.
7. Yaws, C. L.; Richmond, P. C., Chapter 21 - Surface tension—Organic compounds. In *Thermophysical Properties of Chemicals and Hydrocarbons*, Yaws, C. L., Ed. William Andrew Publishing: Norwich, NY, 2009; pp 686-781.
8. Speight, J., *Lange's Handbook of Chemistry, 70th Anniversary Edition*. McGraw-Hill Education: 2005.
9. (a) Borjigin, T.; Sun, F.; Zhang, J.; Cai, K.; Ren, H.; Zhu, G., A microporous metal–organic framework with high stability for GC separation of alcohols from water. *Chem. Commun. (Cambridge, U. K.)* **2012,** *48* (61), 7613-7615; (b) Y., L. J.; S., Y. T.; C., S. J.; C., R., Observations related to tetrahydrofuran and methane hydrates for laboratory studies of hydrate-bearing sediments. *Geochem. Geophys. Geosyst.* **2007,** *8* (6); (c) Kajiwara, T.; Higuchi, M.; Yuasa, A.; Higashimura, H.; Kitagawa, S., One-dimensional alignment of strong Lewis acid sites in a porous coordination polymer. *Chem. Commun. (Cambridge, U. K.)* **2013,** *49* (89), 10459-10461; (d) Fach, E.; Waldman, W. J.; Williams, M.; Long, J.; Meister, R. K.; Dutta, P. K., Analysis of the biological and chemical reactivity of zeolite-based aluminosilicate fibers and particulates. *Environ. Health Perspect.* **2002,** *110* (11), 1087-1096.